

Chapter 3

Structural Studies

X-ray Diffraction Analysis

3.1 X-ray Diffraction Analysis (XRD)

3.1.1 Introduction

X-rays are high energy electromagnetic radiations having energies ranging from 200 eV to 1MeV, which lies between γ -rays and ultraviolet radiation. Their wavelengths are varying from 10 nm to 1 pm. The useful range of x-rays for diffraction studies is between 0.05 nm to 0.25 nm, which is close to inter-atomic spacing (0.2nm) in crystals. X-rays are produced in an X-ray tube having two metal electrodes (tungsten as cathode and Cu or other metal as anode). Electrons which are produced by heating tungsten filament kept at high negative potential, accelerated towards the anode at ground potential. The loss of energy of the electrons due to impact with the metal anode is manifested as X-rays. Only a small percentage (less than 1%) of energy of the electron beam is converted to X-rays, the majority is dissipated as heat in the water-cooled metal anode.

If the incident electron has sufficient energy to eject an electron from inner-shell, the atom will be left in an excited state with a hole in the electron shell. Suppose this hole is created in innermost K shell and if it is filled by an electron from next outer L shell, an X-ray photon with energy equal to the difference in the electron energy levels is produced. L shell contains three sub shells named L_I , L_{II} and L_{III} . Transitions from L_{III} , L_{II} to K results emission of $K\alpha_1$ and $K\alpha_2$ respectively. If the $K\alpha_1$ and $K\alpha_2$ lines cannot be resolved, the characteristic line is simply called the $K\alpha$ line and the wavelength is given by the weighted average of the $K\alpha_1$ and $K\alpha_2$ lines. In our experiment we used Cu source having $K\alpha_1$ (1.5406 nm) and $K\alpha_2$ (1.54439 nm) and weighted average of the $K\alpha_1$ and $K\alpha_2$ is found to be $= \frac{1}{3} (2 \times 1.5406 + 1.54439) = 1.54184$ nm.

3.1.2 X-ray source

Depending on the target metal, suitable operating voltage is required to knock out K electron. In our work instrument operator used 40 kV operating voltage and 30 mA operating current to produce x-ray from copper (Cu) target.

3.1.3 Geometry of X-ray Diffractometer

The three basic components of an x-ray diffractometer are: *x-ray source*, *specimen*, *x-ray detector* and they all lie on the circumference of a circle, which is known as *focusing circle*. The angle between the plane of the specimen and the x-ray source is θ called *the Bragg angle* and the angle between the projection of the x-ray source and the detector is 2θ .

There are four geometries which are used to record X-ray patterns. First geometry is called the θ - 2θ geometry in which the X-ray source is fixed and the detector moves through a range of angles. In the second geometry i.e. θ - θ geometry both the X-ray source and the detector moves in the vertical plane in opposite directions above the centre of the specimen. Two more specialized geometries are called ω geometry and ϕ geometry, are not widely used although very useful. The *diffractometer circle* also referred to as the *goniometer circle* is centered at the specimen, and both the source and the detector lie on the circumference of the circle. The goniometer is the central component of an x-ray diffractometer and contains the specimen holder. It has arms on which the x-ray source and the detector are mounted.

3.1.4 Examination of X-ray diffraction pattern

X-ray diffraction patterns also called reflections which consist of a series of peaks. The peak intensity is plotted on the ordinate (y axis) and the measured diffraction angle, 2θ , along the abscissa (x axis). Each peak in the diffraction pattern corresponds to X-rays diffracted from a specific set of planes in the specimen, and they are of different heights (intensities). The intensity is proportional to the number of X-ray photons of a particular energy counted by the detector for that particular angle 2θ . Since it is difficult to measure absolute value of intensity, it is usually expressed in arbitrary units.

The intensities of the reflections depend on several factors i.e. structure factor, incident intensity, slit width and values of operating voltage and current used in the X-ray source. As-recorded X-ray diffraction patterns generally have a background which is usually subtracted and the peaks are smoothed. The positions of the reflections in an X-ray diffraction pattern depend on the crystal structure (shape and size of the unit cell) of the PbWO_4 . The position of the peak also depends on the wavelength of the X-ray used. The width of an individual peak, often defined as the full width at half the maximum height, can be used to determine crystallite size and the presence of lattice distortions (strain) in the PbWO_4 . For low values of 2θ each reflection appears as a single sharp peak. For larger values of 2θ (above 80°) each reflection consists of a pair of peaks, which correspond to diffraction of the $K\alpha_1$ and $K\alpha_2$ wavelengths. At low 2θ values of the separation of the peaks is quite small, but increases at larger 2θ values. The separation of the $\text{Cu } K\alpha_1$ and $K\alpha_2$ peaks increases from 0.05° at $20^\circ(2\theta)$ to 1.08° at $150^\circ(2\theta)$.

Broadening of X-ray diffraction peaks arises mainly due to three factors:

1. Instrumental effect:

These effects include imperfect focusing, unresolved α_1 and α_2 peaks or if these peaks are resolved then their finite width can cause broadening.

2. Crystallite size:

The peaks become broader due to the effect of small crystallite sizes, and thus analysis of peak broadening can be used to determine the crystallite size. Small crystallite sizes introduce broadening in addition to broadening due to instrumental effect.

Scherrer has derived an expression for broadening of X-ray diffraction peaks only due to small crystallite sizes:

$$B_{crystallite} = \frac{k\lambda}{L \cos\theta}$$

Where,

λ = wavelength of X-ray used

θ = Bragg angle

k = constant between 0.89 to 1.39

3. Lattice strain:

The lattice strain in the material also causes broadening of the diffraction peak, which can be represented by the relationship,

$$B_{strain} = \eta \tan\theta$$

Where, η = strain in the material

3.2 Characterization

3.2.1 Instruments used to record X-ray spectra

We have done XRD characterization of our samples at two centers: One under UGC-CSR Indore Center, M.P. and Other at ERDA, Vadoadara. The XRD measurements were carried out using Bruker D8 Advance X-ray diffractometer installed at the Indore Centre under UGC Consortium for scientific research facility shown in Figure 3.2.1. The standard sample holder of the diffractometer has a 9 sample changer, making it possible to measure up to 9 samples in as series. The diffractometer uses a 1-D position sensitive detector based on silicon drift detector technique which reduces the measurement time significantly without reduction in the diffracted intensity. The maximum global count rate handled by this detector is $\sim 10^8$ cps. The inset in the photograph of the XRD system is the sample holder. The X-rays were produced using a sealed tube and the wavelength of X-ray was 0.154 nm (Cu K-alpha). The X-rays were detected using a fast counting detector based on Silicon strip technology (Bruker LynxEye detector).

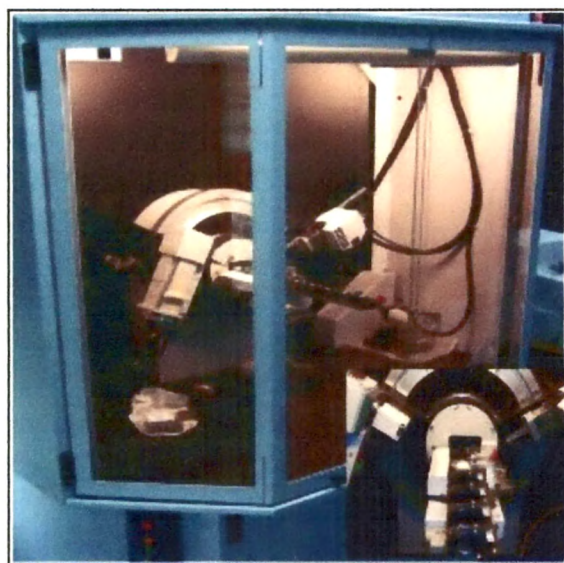


Figure 3.2.1 Photograph of XRD instrument at UGC-CSR, Indore Centre

Powder X-ray diffraction (XRD) patterns of some samples were recorded with a Japan RigakuD/max-RB diffractometer (Figure 3.2.2) in Electrical Research and Development Association (ERDA) at Vadodara with a scanning rate of $3^\circ/\text{min}$ using Cu $K\alpha$ radiation ($\lambda = 0.15406 \text{ nm}$). The operation voltage and current were fixed at 40 kV and 40mA, respectively.



Figure 3.2.2 Photograph of XRD instrument at ERDA, Vadodara

3.2.2 Analysis of XRD data

Analysis of XRD data was done by “PowdeX” program (available free online or can get by e-mail: chengdon@aphy.iphy.ac.cn) provided by Cheng Dong, Institute of Physics, National Laboratory for Superconductivity, Institute of Physics, Chinese Academy of Sciences, Beijing.

3.2.3 Procedure to analysis XRD data with PowderX Program

As obtained XRD file was imported to PowderX program. $K\alpha_2$ elimination was done by DONG’s method. Noise elimination was performed by adaptive smoothing. Background subtraction was performed via Sonneveld method. Lastly Peak search and indexing were done. Path of XRD analysis by PowderX software is shown below.

Data import → $K\alpha_2$ elimination → Smoothing → Background Subtraction → Peak Search → Indexing

3.3 X-ray diffraction analysis of PbWO₄

3.3.1 Introduction

In order to do systematic analysis, we have divided our experiment in to *two parts*. In the first part of our experiment undoped as well as Cerium doped PbWO₄ crystals were synthesized with different Lead sources (Lead Acetate, Lead Nitrate and Lead Chloride) using Hydrothermal Method. In the second part of our experiment PbCl₂ was kept constant as a Lead source and undoped as well as Cerium doped PbWO₄ crystals were produced by varying reaction temperatures and pH of solution. Effect of different lead sources, reaction temperatures and pH of solution on crystal structure and phase were studied by X-ray diffraction analysis technique. Calculation of lattice parameters, unit cell volume and average crystallite size (using Debye-Scherrer formula) were performed in order to determine crystal structure and phase produced for all samples using PowderX program.

3.3.2 Literature Survey

There are hundreds of papers published in which PbO and WO₃ is used as precursor to synthesize large single crystals of PbWO₄ via either Czochralski or Bridgman method. As already discussed in Chapter 1, these methods are expensive and produce harmful gases during crystal growth due to higher synthesis temperature which lowers applicability of these methods for large scale production of PbWO₄ crystals. Moreover, products obtained by these methods are in bulk sized which cannot be used for devices based on nano dimensions. So we have mentioned below only those methods which are effective to produce nanosized PbWO₄ nanomaterial.

According to literature survey, there are 11 papers published on PbWO₄ in which Lead Acetate is used as Lead source to produce PbWO₄ with different morphologies. Out of these eleven papers, 3 papers are based on hydrothermal method [1, 2, 3], 4 papers are based on sonochemical method [4, 5, 6, 7] and 2 paper is based on wet chemical method [8, 9], and two on microemulsion route [10, 11]. In all the published papers mentioned here, pure stolize phase is produced. In our case stolzite phase is produced along with raspite phase. Similarly, there are 9 papers published on PbWO₄ in which Lead Nitrate is used as Lead source. Out of these nine papers only one paper is based on hydrothermal route [12], five papers are based on wet chemical method [13, 14, 15, 16, 17], two on microwave assisted method [18, 19], and one paper on microemulsion method [20]. Only one paper by Changhua An [12] had been reported so far in which Lead Chloride is used as Lead source to produce PbWO₄.

3.3.3 Synthesis of PbWO_4 with different Lead Sources

In the first part of experiment various compounds of Lead [$\text{Pb}(\text{CH}_3\text{COO})_2$, $\text{Pb}(\text{NO}_3)_2$, PbCl_2] were used as Lead source and Na_2WO_4 was taken as second reagent. Lead sources, $\text{Na}_2\text{WO}_4 \cdot 2\text{H}_2\text{O}$ and CeO_2 purchased from Alfa Aesar were analytical reagent grade purity. Distilled water was used as solvent to prepare all required solutions. Initially 30 ml solution of 0.01 M concentration of $\text{Pb}(\text{CH}_3\text{COO})_2$ was prepared by continuous stirring with magnetic needle in a glass bowl A. 30 ml solution of 0.01 M concentration of Na_2WO_4 was also prepared separately in another glass bowl B. Both these salts are well dissolved in distilled water and produce transparent solutions. Thus prepared solution of Na_2WO_4 from the glass bowl B is added drop wise in the glass bowl A. Instantly white precipitates of PbWO_4 were formed. In order to dope Cerium, 0.001M solution of CeO_2 was prepared in third glass bowl C and added drop wise to the glass bowl A. As prepared solution from the glass bowl A was transferred to Teflon Lined Stainless Steel Autoclave and filled upto 80% of its maximum capacity. Autoclave was put on hot plate to achieve desired temperature and time of reaction. After achieving required temperature and time for reaction autoclave is air cooled to room temperature. Obtained white precipitates were washed several times with absolute ethanol and filtered with Wattman fine filter papers to remove unwanted extra salt. After removing unwanted salt, to remove the water content, white powder was dried in vacuum oven at 80°C for 2h. Similar products were also obtained by using $\text{Pb}(\text{NO}_3)_2$ and PbCl_2 as Lead sources. Preparation conditions and chemical reactions of above experiment are given below in tabulated form in Table 3.1. XRD reflection spectra of thus obtained samples are shown in Figure 3.3.1 and Figure 3.3.2.

The reaction processes can be expressed as follow:

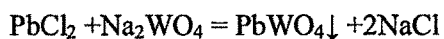
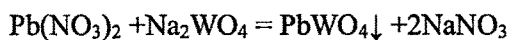
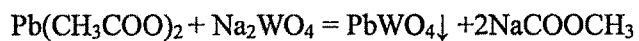


Table 3.1 Summary of reaction conditions to synthesize PbWO_4 and $\text{PbWO}_4:\text{Ce}$ using different Lead sources.

Sample	Reagent1 conc. (0.01M)	Reagent2 conc. (0.01M)	Dopant conc. (0.001M)	Solvent	Temp. (°C)	Time (h)
1	$\text{Pb}(\text{CH}_3\text{COO})_2$	Na_2WO_4	-	D.W.	100	12
2	$\text{Pb}(\text{CH}_3\text{COO})_2$	Na_2WO_4	CeO_2	D.W.	100	12
3	$\text{Pb}(\text{NO}_3)_2$	Na_2WO_4	-	D.W.	100	12
4	$\text{Pb}(\text{NO}_3)_2$	Na_2WO_4	CeO_2	D.W.	100	12
5	PbCl_2	Na_2WO_4	-	D.W.	100	12
6	PbCl_2	Na_2WO_4	CeO_2	D.W.	100	12

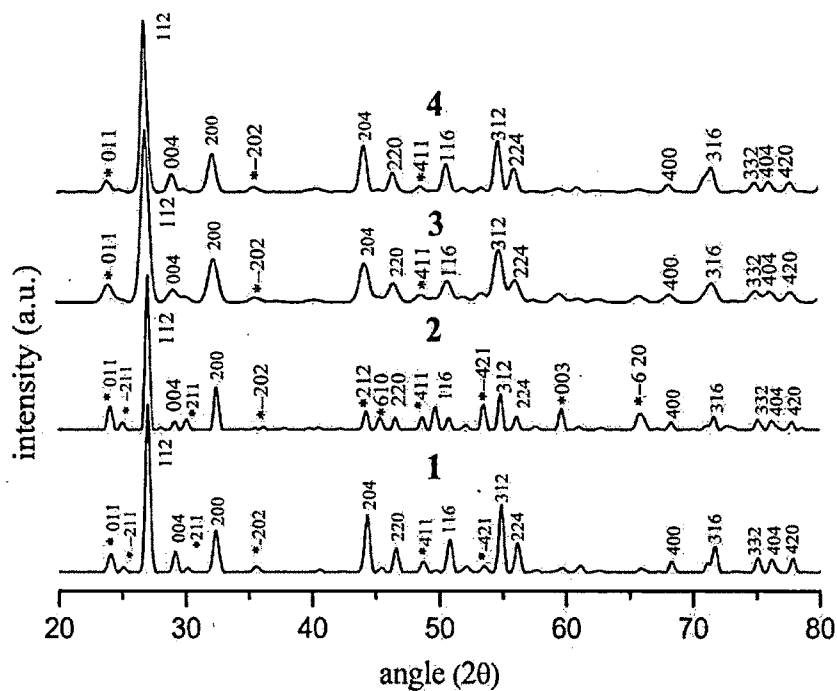


Figure 3.3.1 XRD reflections of undoped and Cerium doped PbWO_4 synthesized using Lead Acetate (1, 2) and Lead Nitrate (3,4).

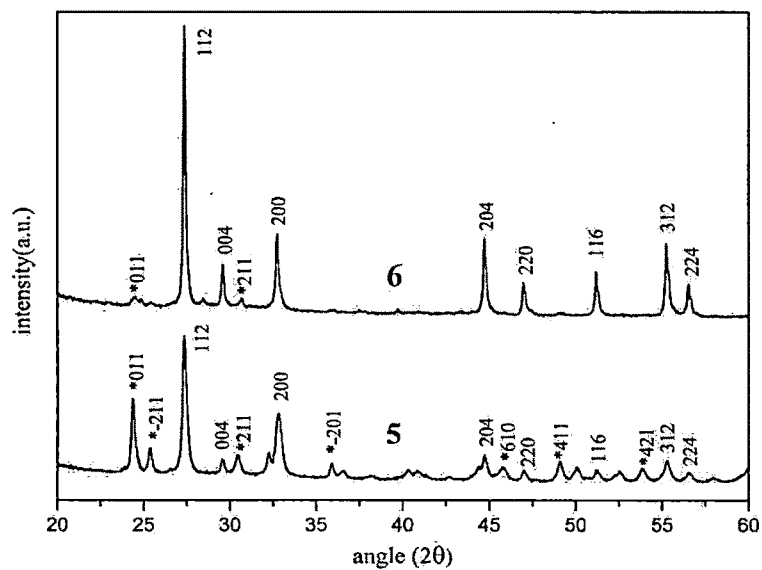


Figure 3.3.2 XRD reflections of undoped and Cerium doped PbWO_4 synthesized using Lead Chloride (5,6).

Table 3.2 Summary of phase, lattice parameters, unit cell volume and average crystallite size of undoped and Cerium doped PbWO_4 .

Sample No.	Reagent 1 conc. (0.01M)	Reagent 2 conc. (0.01M)	Dopant conc. (0.001M)	Phase	Lattice Parameter (Å)			Volume (Å) ³	Average Crystallite size (nm)
					a	b	c		
1	$\text{Pb}(\text{CH}_3\text{COO})_2$	Na_2WO_4	-	stolzite	5.5890	5.5890	12.030	375.78	19.08
				raspite	13.655	4.9760	5.5601	375.08	
2	$\text{Pb}(\text{CH}_3\text{COO})_2$	Na_2WO_4	CeO_2	stolzite	5.5730	5.5730	12.028	373.56	18.60
				raspite	13.555	4.9750	5.5601	374.95	
3	$\text{Pb}(\text{NO}_3)_2$	Na_2WO_4	-	stolzite	5.6445	5.6445	12.047	383.82	19.89
				raspite	13.580	4.9900	5.5600	376.76	
4	$\text{Pb}(\text{NO}_3)_2$	Na_2WO_4	CeO_2	stolzite	5.5478	5.5478	12.025	370.10	19.45
				raspite	13.561	4.9770	5.5610	375.32	
5	PbCl_2	Na_2WO_4	-	stolzite	5.4637	5.4637	12.042	359.47	28.27
				raspite	13.561	4.9760	5.5601	375.19	
6	PbCl_2	Na_2WO_4	CeO_2	stolzite	5.4630	5.4630	12.040	359.32	42.81
				raspite	13.530	4.977	5.5610	374.47	

3.3.4 Effect of Lead Sources

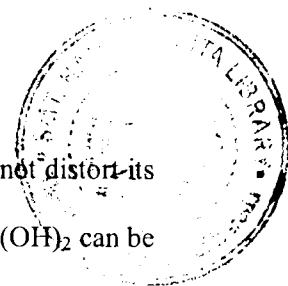
Figure 3.3.1 shows typical X-ray diffraction pattern of as synthesized PbWO_4 (samples 1 and 3) and Cerium doped PbWO_4 (samples 2 and 4) in which $\text{Pb}(\text{CH}_3\text{COO})_2$ and $\text{Pb}(\text{NO}_3)_2$ were used as Lead sources, respectively. Similarly, Figure 3.3.2 shows X-ray diffraction pattern of PbWO_4 (sample 5) and cerium doped PbWO_4 (sample 6) in which PbCl_2 was used as a Lead source. Both Figures are recorded with different instruments at different scanning rate, hence shown separately. The peak intensity is plotted on the ordinate (y axis) and the diffraction angle, 2θ , along the abscissa (x axis). Each peak also called *reflection*, in the diffraction pattern corresponds to X-ray diffracted from a specific set of planes of PbWO_4 crystal lattice. Each reflection has different intensity (rather relative intensity) which is proportional to the number of X-ray photons of a particular energy counted by detector for each angle 2θ .

X-ray reflection spectra (Figure 3.3.1 and Figure 3.3.2) reveals that all prepared samples are polycrystalline in nature and contains two phases of PbWO_4 . All X-ray diffraction peaks were indexed to a tetragonal scheelite (stolzite) phase with space group $I4_1/a$ and monoclinic raspite phase with space group $P2_1/a$. The peaks representing raspite phase are marked with symbol (*) for all samples. The formation of Tungstic acid ($\text{H}_2\text{WO}_4 \cdot n\text{H}_2\text{O}$), other tungsten oxide hydrates ($\text{WO}_3 \cdot n\text{H}_2\text{O}$) and unwanted impurity of Na_2WO_4 , $\text{Ce}_2(\text{WO}_4)_3$, PbO , and $\text{Pb}(\text{OH})_2$ were not observed. Calculation of lattice parameters, unit cell volume and average crystallite size were performed for individual sample using Scherrer formula with the help of PowderX software and given in Table 3.2. The highest relative intensity is obtained for (1 1 2) crystallographic plane of tetragonal crystal structure or stolzite phase.

As discussed in Chapter 1, in the tetragonal stolzite structure, W atoms are in tetrahedral O-atom cages and isolated from each other, whereas in monoclinic raspite structure, two W atoms share two O atoms to form a chain of edge-shared octahedra. Each Pb ion is surrounded by seven O ions in the raspite structure, whereas in the scheelite structure, the number of the surrounding O ions to each Pb ion is eight. The monoclinic form of PbWO_4 (raspite-type) can be considered as a distortion of the tetragonal form of PbWO_4 (scheelite-type). As raspite phase is transform irreversibly to stolzite phase at higher temperature, high temperature solid state reactions produce PbWO_4 crystals having pure stolzite phase. XRD data analysis confirms the presence of raspite phase in all the samples. This indicates that at low temperature raspite phase is produced predominantly and with increase in temperature it transforms irreversibly into stolzite phase. Hence some inclusions of raspite phase are still present at 100°C reaction temperature denoted by (*).

Using $\text{Pb}(\text{CH}_3\text{COO})_2$ as a Lead source, large amount of raspite phase was produced when compared to $\text{Pb}(\text{NO}_3)_2$ and PbCl_2 . It should be noted that PbWO_4 prepared with Lead Chloride contains least amount of raspite phase inclusions. Efforts are made to find the reason for the well observed raspite phase due to $\text{Pb}(\text{CH}_3\text{COO})_2$ required more experimental evidence.

Comparing Figure 3.3.1 and Figure 3.3.2, it is observed that among all, sample 5 and sample 6 shows high crystallinity. Hence Lead Chloride proved to be better Lead source to produce high crystalline PbWO_4 crystals over Lead Nitrate and Lead Acetate.



XRD reflection spectra also confirm that Cerium doping in PbWO_4 does not distort its characteristic shape. No other impurities such as $\text{Ce}_2(\text{WO}_4)_3$, PbO and $\text{Pb}(\text{OH})_2$ can be observed and it reveals that the doping of Ce^{3+} at different temperatures does not change the crystal structure or induce a new phase. The Ce^{3+} ions are likely to enter PbWO_4 crystal lattice to substitute Pb^{2+} sites considering that the ion radius of Ce^{3+} (0.103 nm) is similar to that of Pb^{2+} (0.120 nm) [21]. Figure 3.3.2 shows that intensity of raspite phase peaks are greatly suppressed by Cerium doping. This type of peak suppression is not observed in Figure 3.3.1. Reason of this interesting phenomenon is not clear but we can simply conclude that Cerium act as catalyst and helps raspite phase to convert into stolzite phase when Lead Chloride was used as Lead source.

The volumes of the unit cells of these two structures are very close; the difference is less than 0.53% which can be seen from Table 3.2. Range of unit cell volume for stolzite phase is 359.47-383.83 (\AA)³ and that is for raspite phase is 359.09-375.32 (\AA)³. The average crystallite sizes were estimated by the Scherrer's equation using the full width at half maximum (FWHM) of the most intense peak (1 1 2). The average crystallite size calculated using the Debye-Scherrer formula given in the literature [21], described as follows,

$$D = \frac{k\lambda}{\beta \cos \theta}$$

Where D is the average crystallite size or particle size, k is the constant equal to 0.94, λ is the wavelength of the X-rays equal to 0.1542 nm, θ is the Bragg angle and β is FWHM. Value of average crystallite size are smaller for PbWO_4 prepared using Lead Acetate and Lead Nitrate compared to that of prepared using Lead Chloride. Due to small crystallite size, the number of parallel planes available is too small for a sharp diffraction maximum to build up and hence the reflection peaks in the diffraction

pattern becomes broadened for sample 1 to 4 (Figure 3.3.1) while it is sharp for sample 5 and 6 (Figure 3.3.2). Cerium doping reduce the crystallite size in the case of $\text{Pb}(\text{CH}_3\text{COO})_2$ or $\text{Pb}(\text{NO}_3)_2$ while it is increase in the case of PbCl_2 as a Lead source.

According to the Bragg equation, the shift of reflection peaks towards higher angle suggests the decrease in lattice parameter of as-synthesized products. In order to confirm this we have magnified scale of characteristic reflection peak (112) of all PbWO_4 samples and compare the shift with calculated lattice parameter in Table 3.2.

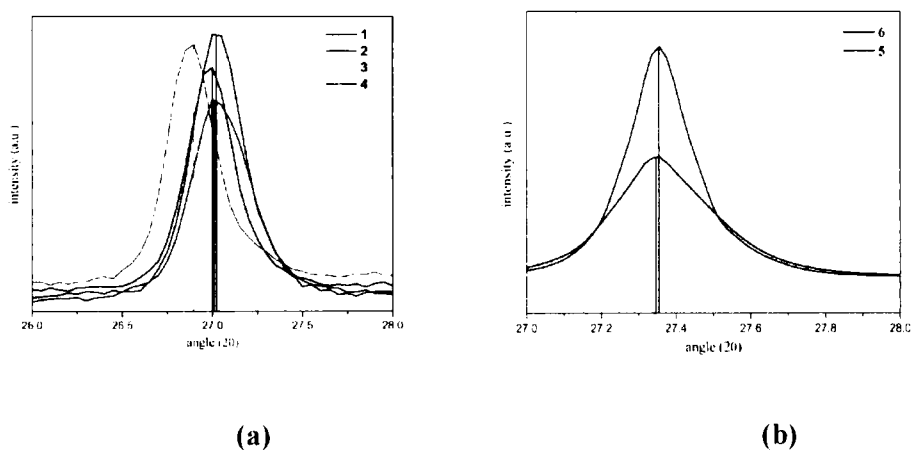


Figure 3.3.3 Magnified (112) reflection peak of (a) Sample 1-4 (b) Sample 5-6

Figure 3.3.3 (a) and (b) are the images of characteristic (112) reflection peak of PbWO_4 on magnified scale. In Figure 3.3.3 (a) and (b) peak position of Cerium doped samples (2, 4 and 6) are shifted to higher angle compared to that of undoped sample (1, 3 and 5). The shift of reflection peaks towards higher angle suggests the decrease in lattice parameter can be seen in Table 3.2. As already mentioned Ce^{3+} substitute well Pb^{2+} in PbWO_4 lattice and induce Pb^{2+} vacancy in order to keep the charge neutral. The substitution of Ce^{3+} ion with ionic radius (0.103 nm) is slightly smaller than that of Pb^{2+} (0.120 nm) [22] which also explain our result reported [23, 24].

3.4 Lead Chloride as a Lead Source

Lead Chloride (PbCl_2) is an inorganic compound which is a white solid under ambient conditions. Lead Chloride is one of the most important lead-based reagents. It also occurs naturally in the form of the mineral *cotunnite*.

In the first part of our experiment we observed that PbWO_4 with highest crystallinity can be formed by using PbCl_2 as a Lead source. It is also expected that alkali halide compounds produce good luminescence will see in Chapter 5. As mentioned earlier, only one literature is available in which PbWO_4 were synthesized using PbCl_2 is reported till today. These are the some points which encourage us to do systematic research in this direction which is presented in below sections.

3.4.1 Reaction parameters

In this part of experiment Lead Chloride (PbCl_2) was used as Lead source and remaining reagents and synthesis procedure were kept similar to that of previous part. PbWO_4 synthesized at different Temperature and by varying pH of solvent, taking 0.01 M concentration of PbCl_2 , Na_2WO_4 and 0.001M concentration of CeO_2 . All these experiments in which Lead Chloride was used as Lead source are summarized and tabulated in Table 3.3.

Table 3.3 PbWO₄ and PbWO₄:Ce prepared at different reaction conditions using Lead Chloride as a Lead source.

Sample No.	PbCl ₂ conc. (M)	Na ₂ WO ₄ conc. (M)	Ce conc. (M)	Temp. (°C)	Time (h)	pH
5	0.01	0.01	-	100	10	7
6	0.01	0.01	0.001	100	10	7
7	0.01	0.01	-	125	10	3
8	0.01	0.01	-	125	10	7
9	0.01	0.01	-	125	10	11
10	0.01	0.01	-	150	10	7
11	0.01	0.01	0.001	150	10	7
12	0.01	0.01	-	200	10	7
13	0.01	0.01	0.001	200	10	7
14	0.01	0.01	0.001	R.T.	10	7

3.5 Effect of pH of reaction solution on PbWO₄

The pH of reaction system is one of the most important factors. It has been found that the pH value of the precursor medium plays an important role in the formation of tungstate phase and their morphology. Controlled experiments were carried out to investigate the influence of pH on the synthesis of PbWO₄.

To study the effects of pH of solvent on structural properties of PbWO₄ was prepared with 3pH, 7pH and 11pH and they denoted by sample 7, 8 and 9 as shown in Table 3.4. During preparation of sample 7, pH of distilled water was set to 3 by adding Acetic acid (Glacial) (CH₃COOH) drop wise while pH of distilled water was increased up to 11 by adding Sodium Hydroxide (NaOH) for sample 9. In all this experiments temperature was kept at 125° C and synthesis time was kept for 10 h.

Table 3.4 PbWO₄ prepared with different pH of reaction solution

Sample	PbCl ₂ conc. (M)	Na ₂ WO ₄ conc. (M)	Temp. (°C)	Time (h)	pH
7	0.01	0.01	125	10	3
8	0.01	0.01	125	10	7
9	0.01	0.01	125	10	11

Figure 3.5.1 (a), (b) and (c) shows the XRD pattern of PbWO₄ powders synthesized at different pH 3, 7 and 11, respectively. The XRD data files for these samples are treated with by PowderX software and Indexed images are shown below.

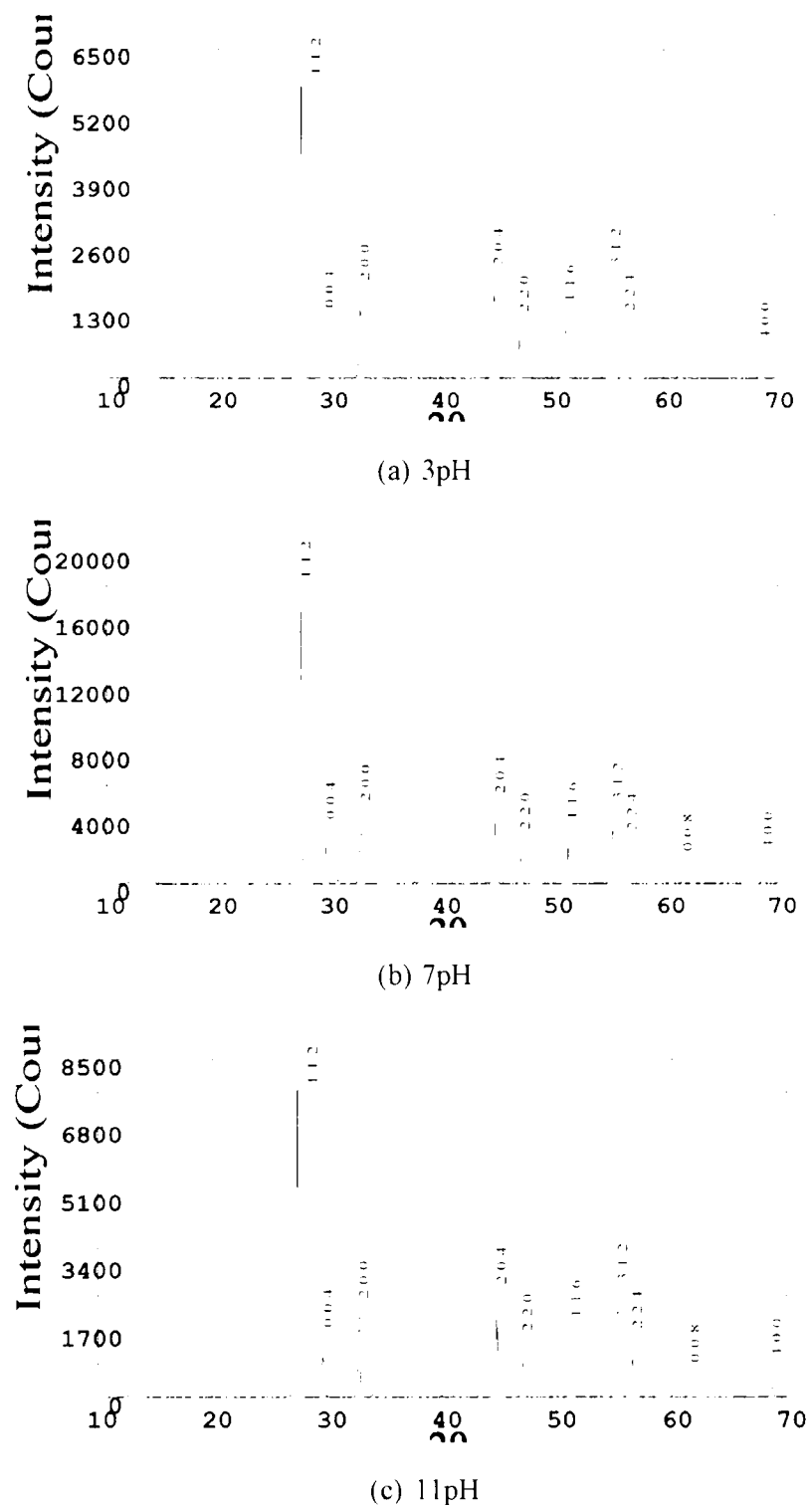


Figure 3.5.1 Indexed XRD reflections of PbWO₄ synthesized at (a) 3pH, (b) 7pH and (c) 11pH. (Images from PowderX program)

It can be seen from the Figure 3.5.1 (a), (b) and (c) that PbWO_4 synthesized at different pH of reaction solution is a single phase. All the reflection peaks can be completely indexed to a pure tetragonal stolzite phase of PbWO_4 with space group $I4_1/a$. The formation of Tungstic acid $\text{H}_2\text{WO}_4 \cdot n\text{H}_2\text{O}$, other tungsten oxide hydrates $\text{WO}_3 \cdot n\text{H}_2\text{O}$ and unwashed impurity of Na_2WO_4 washed not observed. XRD results indicate that the powders are free of secondary phases. The strong and sharp peaks indicate that the PbWO_4 powders processed in 3pH, 7pH and 11pH are highly crystallized and structurally ordered at long-range. This result shows that the different pH promotes the formation of crystalline PbWO_4 powders at low synthesis temperature and reduced processing time than the other conventional methods.

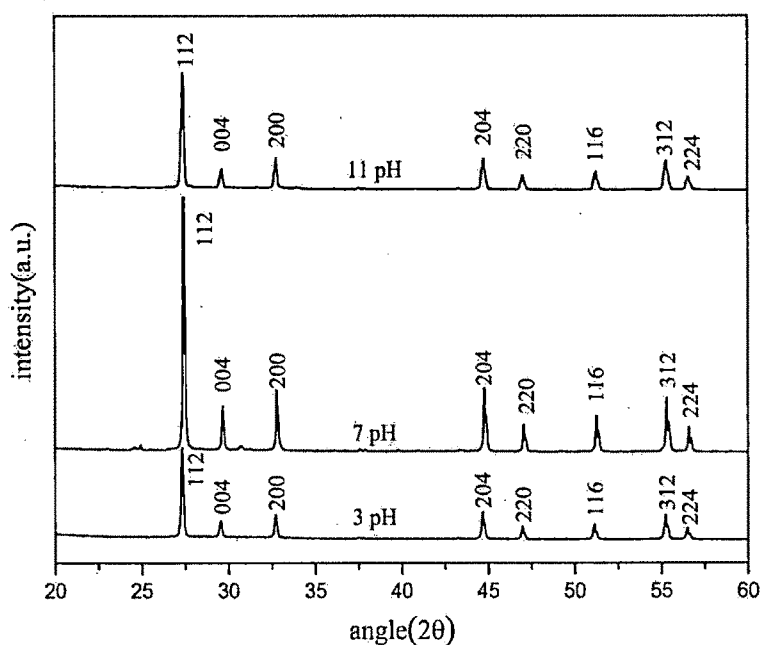


Figure 3.5.2 XRD pattern of PbWO_4 prepared at different pH

However, on comparing the XRD spectra of three samples (see Figure 3.5.2), we found that the relative intensity of the peaks varied significantly, which indicates different percentage of crystallinity. Highest crystallization observed for PbWO_4 prepared at 7pH and lowest crystallization observed for PbWO_4 prepared at 3pH. Samples prepared at 7pH and 11pH show better crystallization than the one made at 3pH.

According to Jun Geng et al. [25], 5-9 pH range is optimal for production of PbWO_4 with different morphologies. If the pH value is higher than 11, another complex, $\text{Pb}(\text{OH})_x^{2-x}$, was formed due to the high concentration of OH^- and the strong complexing ability between Pb^{2+} and OH^- . In this case, no product of PbWO_4 could be obtained. But our result shows that PbWO_4 nanomaterials with good crystallinity can be formed even at 11pH and optimal pH range is 3-11 pH.

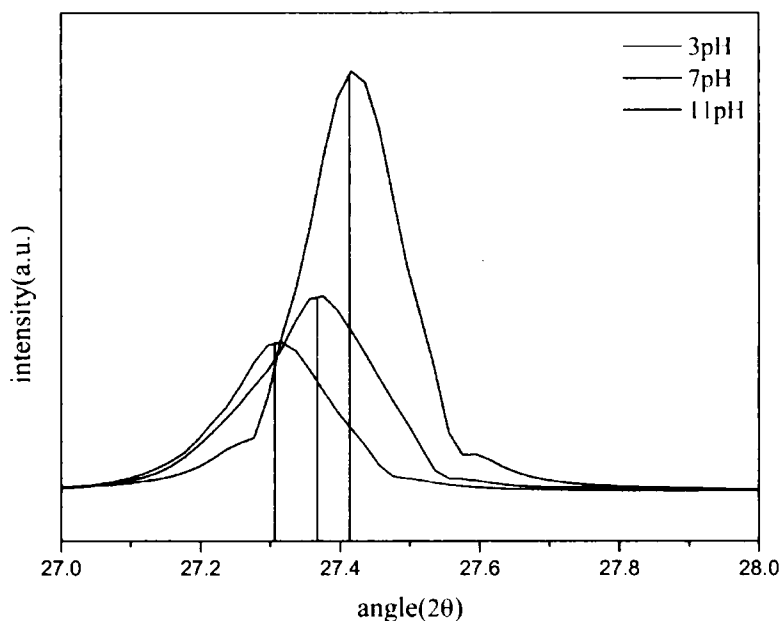


Figure 3.5.3 Shift of (112) reflection peak of PbWO_4 prepared at different pH.

Shift in the main reflection peak (112) of stolzite phase of PbWO_4 is compared and shown in Figure 3.5.3. It can be seen from the figure that (112) peak for sample prepared at 3 pH is at lowest angle and that of for sample prepared at 7pH is at highest angle. According to the Bragg equation, the shift toward higher angle of reflection peaks suggested that the cell parameters of as-synthesized products could continuously decrease. By observing the variation of PowderX calculated lattice parameters for all three sample (Table 3.5) verification of this rule can be done.

Table 3.5 Summary of phase identified, lattice parameters, unit cell volume and average crystallite size of PbWO_4 prepared at different pH.

Sample	pH	Phase	Lattice Parameter (Å)			Volume (Å) ³	Average Crystallite size (nm)
			a	b	c		
7	3	stolzite	5.4614	5.4614	12.046	359.29	40.75
8	7	stolzite	5.4590	5.4590	12.042	358.85	44.75
9	11	stolzite	5.4598	5.4598	12.045	359.05	35.45

3.6 Effect of synthesis Temperature on PbWO₄

Temperature is another most important reaction parameter which controls the crystal structure and morphology of the product. Hydrothermal method is used to produce high crystalline samples at lower synthesis temperature compared to other high temperature solid state reaction. In Hydrothermal method product is in polycrystalline form while High temperature methods are used to produce large single crystals. Low temperature formation of highly crystalline powder products could be used in nano-functional devices.

To study the effect of reaction temperature on crystal structure and phase formation of PbWO₄, samples were synthesized at four different temperatures: 100°C, 125°C, 150°C and 200°C and symbolized as sample 5, 8, 10 and 12, respectively. Preparation condition of sample 5, 8, 10 and 12 are given in Table 3.6.

Table 3.6 PbWO₄ synthesized at different reaction temperatures.

Sample	PbCl ₂ conc. (M)	Na ₂ WO ₄ conc. (M)	Ce conc. (M)	Temp. (°C)	Time (h)	pH
5	0.01	0.01	-	100	10	7
8	0.01	0.01	-	125	10	7
10	0.01	0.01	-	150	10	7
12	0.01	0.01	-	200	10	7

The XRD reflection spectra of PbWO_4 synthesized at different temperatures are shown in Figure 3.6.1. As mentioned earlier, all XRD reflection peaks are indexed to a tetragonal scheelite (stolzite) phase with space group $I4_1/a$ and monoclinic raspite phase with space group $P2_1/a$. The identification of raspite phase peaks for all samples are marked with symbol (*). The formation of Tungstic acid $\text{H}_2\text{WO}_4 \cdot n\text{H}_2\text{O}$, other tungsten oxide hydrates $\text{WO}_3 \cdot n\text{H}_2\text{O}$ and unwanted impurity of Na_2WO_4 , $\text{Ce}_2(\text{WO}_4)_3$, PbO , and $\text{Pb}(\text{OH})_2$ were not observed. XRD spectra of sample 5, 10 and 12 indicates the presence of secondary raspite phase of PbWO_4 while sample 8 is free of secondary phase and contains pure stolzite phase.

Comparing XRD graph of PbWO_4 samples prepared at 100°C , 125°C , 150°C and 200°C following observations can be done. PbWO_4 prepared at 100°C temperature contains highest amount of raspite phase compared to samples prepared at 150°C and 200°C temperatures. With increase of temperature from 100°C to 200°C percentage of raspite phase of PbWO_4 decreases. Among all the samples prepared at different temperatures, pure stolzite phase produced only for sample prepared at 125°C with highest crystallinity. However, on comparing the XRD peaks of the products, we found that the relative intensity of the peaks varied significantly, indicate that at different temperature PbWO_4 with different crystallinity form. Thus different reaction temperature in our experiment would bring about significant changes in the crystallization of stolzite phase of PbWO_4 .

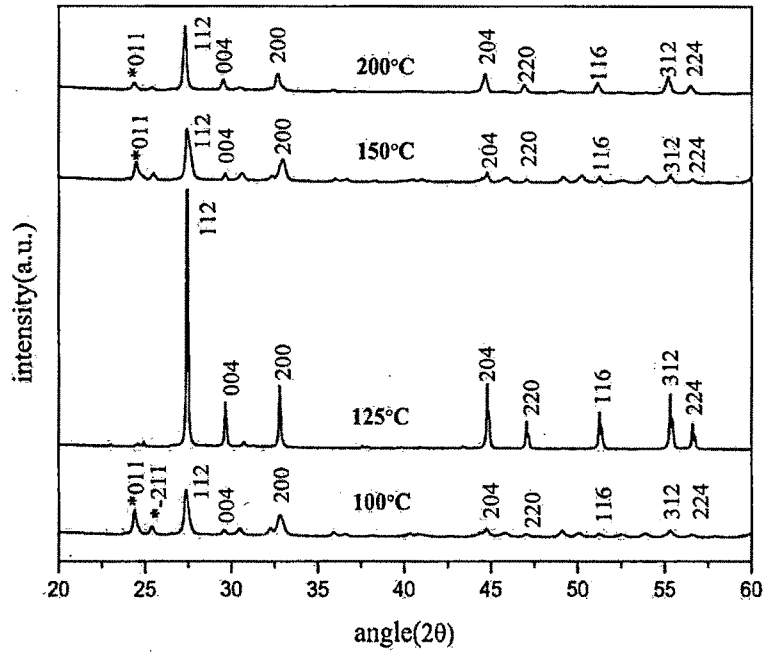


Figure 3.6.1 XRD pattern of PbWO_4 prepared at different Temperature.

Table 3.7 Summary of phase identified, lattice parameters, unit cell volume and average crystallite size of PbWO_4 prepared at different Temperature.

Sample	Temp. (°C)	Phase	Lattice Parameter(Å)			Volume (Å) ³	Average crystallite size (nm)
			a	b	c		
5	100	stolzite	5.4637	5.4637	12.042	359.48	28.27
		raspite	13.561	4.976	5.5601	375.09	
8	125	stolzite	5.4598	5.4598	12.042	358.96	44.75
10	150	stolzite	5.4584	5.4584	12.057	359.23	24.76
		raspite	13.496	4.985	5.579	375.34	
12	200	stolzite	5.4602	5.4602	12.049	359.23	36.32
		raspite	13.552	4.985	5.563	375.82	

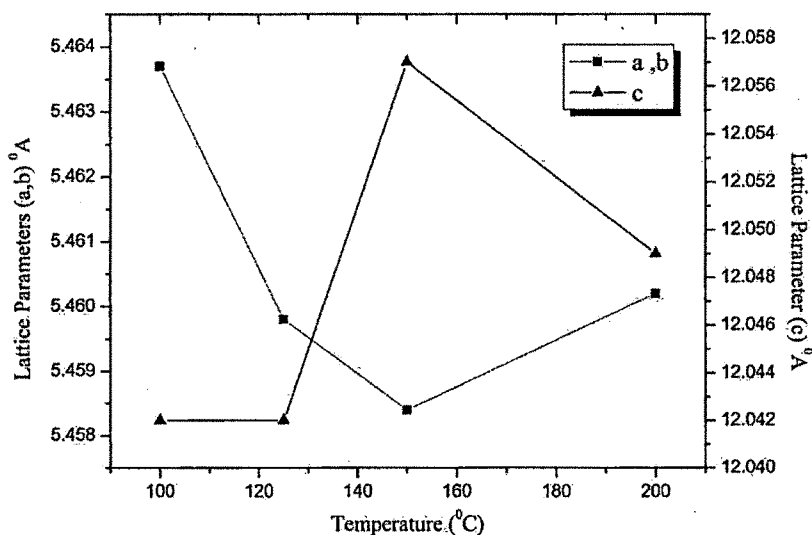


Figure 3.6.2 Effect of synthesis Temperature on Lattice Parameters of PbWO₄

We have plot the graph which shows the variation of lattice parameters of stolzite phase as a function of Temperature. Figure 3.8 shows graph of Temperature verses lattice parameter by taking the values tabulated in Table 3.7. As we can see from the table that, all PbWO₄ samples except prepared at 125 °C, exhibit little amount of raspite phase. Lattice parameter (a, b) is highest for sample prepared at 100 °C which decreases with increase in temperature up to 150 °C and again increase for sample prepared at 200°C. While lattice parameter (c) remains constant for sample prepared at 100 °C to 125 °C and increase and become maximum for 150 °C then again decrease for sample prepared at 200°C.

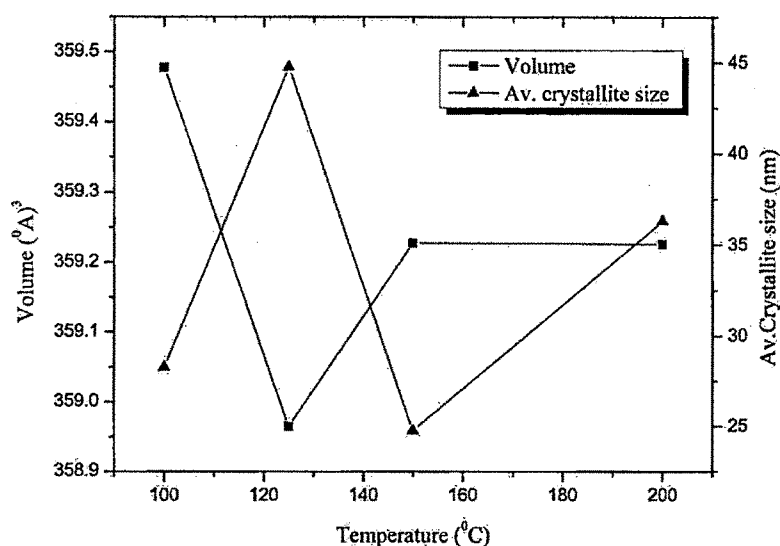


Figure 3.6.3 Effect of synthesis Temperature on Volume and Average Crystallite size of PbWO_4

We have also plot the graph which shows the variation of unit cell volume and average crystallite size as a function of Temperature. Figure 3.6.3 shows the graph of Temperature verses unit cell volume and average crystallite size by taking the values tabulated in Table 3.7. Unit cell volume is highest for sample prepared at 100 °C which decreases with increase in temperature up to 125 °C and again increase for sample prepared at 150°C. This behavior can be associated with aggregates production and nuclei formation [27], promoting the expansion of cell volume. Unit cell volume then remains constant up to 200 °C. While average crystallite size is highest for sample prepared 125 °C and decrease for 150 °C then again increase for sample prepared at 200°C. From the graphs we can conclude that unit cell volume is inversely proportional to average crystallite size.

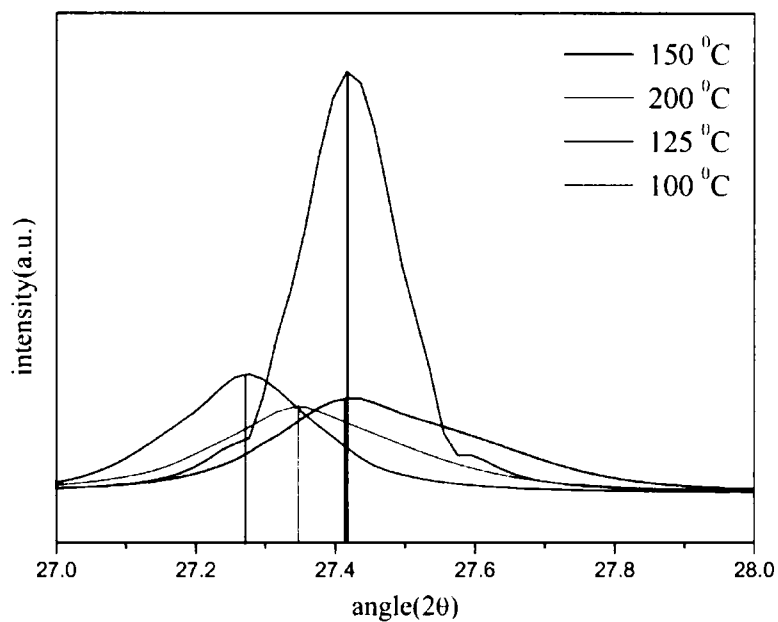


Figure 3.6.4 Shift of (112) peak of PbWO₄ synthesized at different temperature

Figure 3.6.4 shows the shift of reflection peak (112) for different temperature towards higher angle suggests that the cell parameters of as-synthesized products could decrease with Ce³⁺ doping. The peak position of the PbWO₄ samples synthesized at 125°C and 150°C is almost same so lattice parameters of these samples should close to each other and smaller than the sample prepared at 100°C and 200°C. This can be verified by values given in Table 3.7.

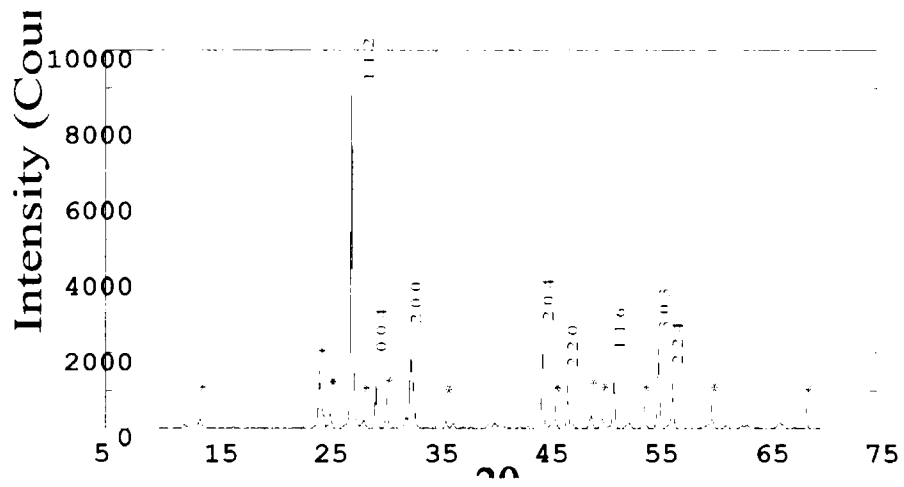
3.7 Effect of synthesis Temperature on PbWO₄:Ce

To study the effect of reaction temperature on crystal structure and phase formation of Cerium doped PbWO₄, PbWO₄ phosphor synthesized at room temperature, 100°C, 150°C and 200°C temperatures were selected and symbolized as sample 6, 11, 13 and 14, respectively. Preparation conditions for sample 6, 11, 13 and 14 are given in Table 3.8.

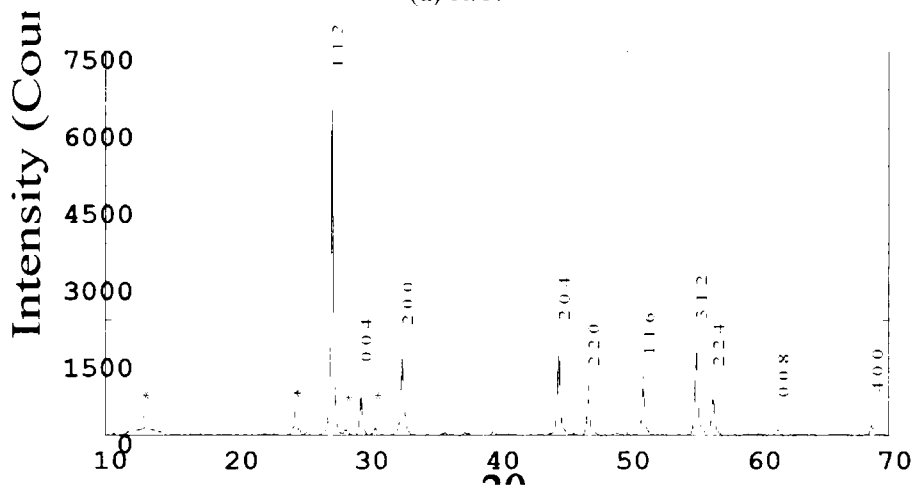
Table 3.8 PbWO₄:Ce synthesized at different reaction temperatures.

Sample	PbCl ₂ conc. (M)	Na ₂ WO ₄ conc. (M)	Ce conc. (M)	Temp. (°C)	Time (h)	pH
6	0.01	0.01	0.001	100	10	7
11	0.01	0.01	0.001	150	10	7
13	0.01	0.01	0.001	200	10	7
14	0.01	0.01	0.001	R.T.	10	7

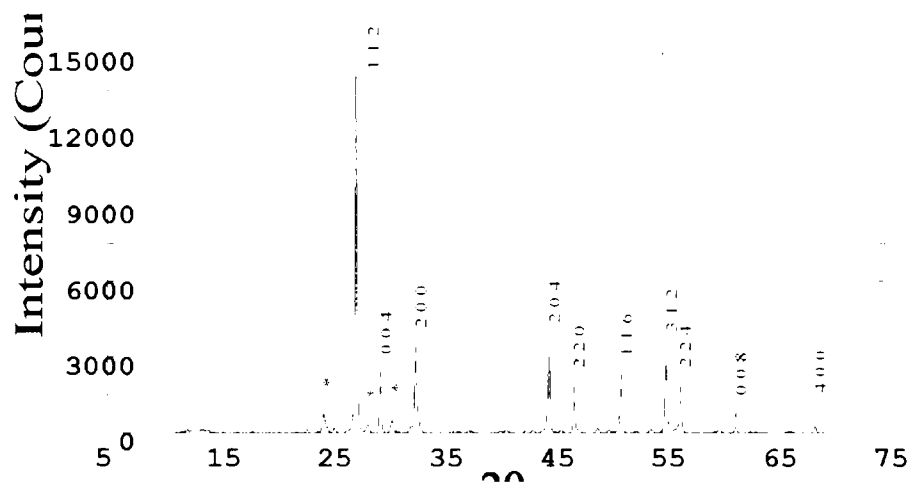
XRD reflection spectra of Cerium doped samples synthesized at room temperature, 100°C, 150°C and 200°C temperatures are refined with PowderX software and shown in Figure 3.7.1 (a), (b), (c) and (d). All XRD reflection peaks are indexed to a tetragonal scheelite (stolzite) phase with space group I4_{1/a} and monoclinic raspite phase with space group P2_{1/a}. The identification of raspite phase peaks for all samples are marked with symbol (*). The formation of Tungstic acid H₂WO₄.nH₂O, other tungsten oxide hydrates WO₃.nH₂O and unwashed impurity of Na₂WO₄ Ce₂(WO₄)₃, PbO and Pb(OH)₂ were not observed in all the samples.



(a) R.T.



(b) 100°C



(c) 150°C

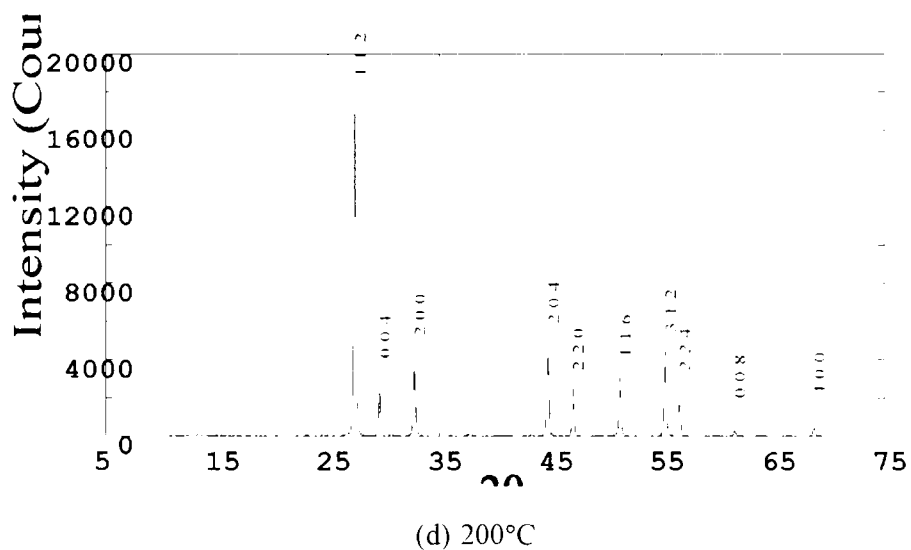


Figure 3.7.1 Indexed XRD spectra of PbWO₄: Ce synthesized at (a) R.T. (b) 100°C (c) 150°C and (d) 200°C.

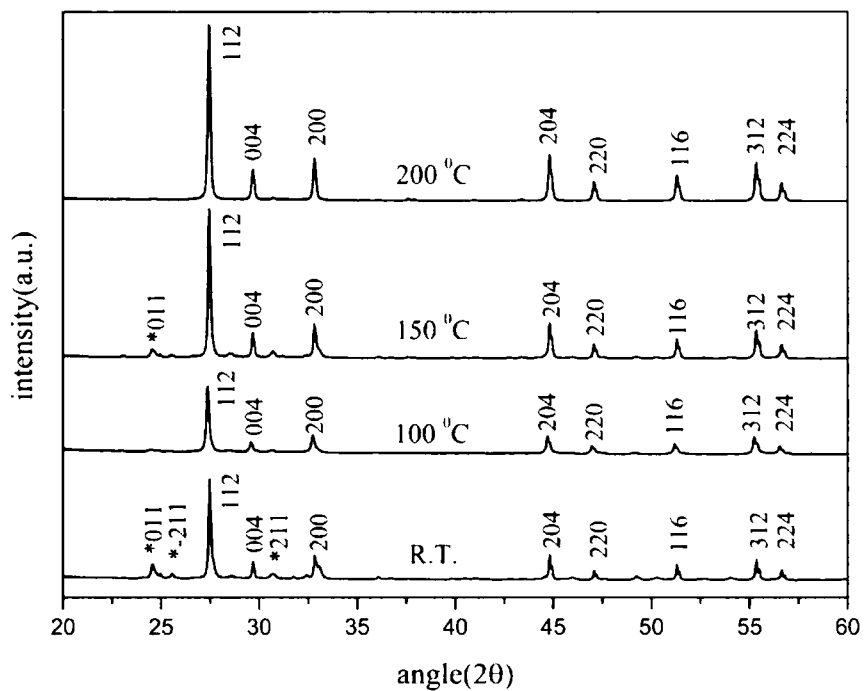


Figure 3.7.2 XRD pattern of PbWO₄:Ce prepared at different Temperature

Table 3.9 Summary of phase identified, lattice parameters, unit cell volume and average crystallite size of $\text{PbWO}_4:\text{Ce}$ prepared at different Temperature.

Sample	Temp. (°C)	Phase	Lattice Parameter(Å)			Volume (Å) ³	Average crystallite size (nm)
			a	b	c		
6	100	stolzite	5.4630	5.4630	12.051	359.65	42.81
		raspite	13.561	4.977	5.561	375.33	
11	150	stolzite	5.4595	5.4595	12.042	358.92	47.82
		raspite	13.555	4.976	5.561	375.09	
13	200	stolzite	5.4596	5.4596	12.042	358.94	46.78
14	R.T.	stolzite	5.4692	5.4692	12.064	360.86	46.77

As we can see from the PowderX refined XRD reflections that relative intensity of XRD peaks are increases as temperature increases from 100°C to 200°C. However, on comparing the intensities of the products, we found that the relative intensity of the peaks varied significantly, which indicates that at different temperature PbWO_4 with different crystallinity form. On doping with Cerium in PbWO_4 , intensity of peaks representing raspite phase decreases, which means that doping of cerium also decrease the amount of raspite phase with increase in temperature. XRD spectra of $\text{PbWO}_4:\text{Ce}$ crystals prepared at 200°C temperature shows raspite free pure stolzite phase. Among all the samples prepared at different temperatures, sample prepared at 200°C is highest crystalline in nature. Intensity of peaks representing stolzite phase also increases with Cerium which can be seen from XRD reflections. These results indicate that along with Temperature, Cerium also plays an important role to increase crystallinity.

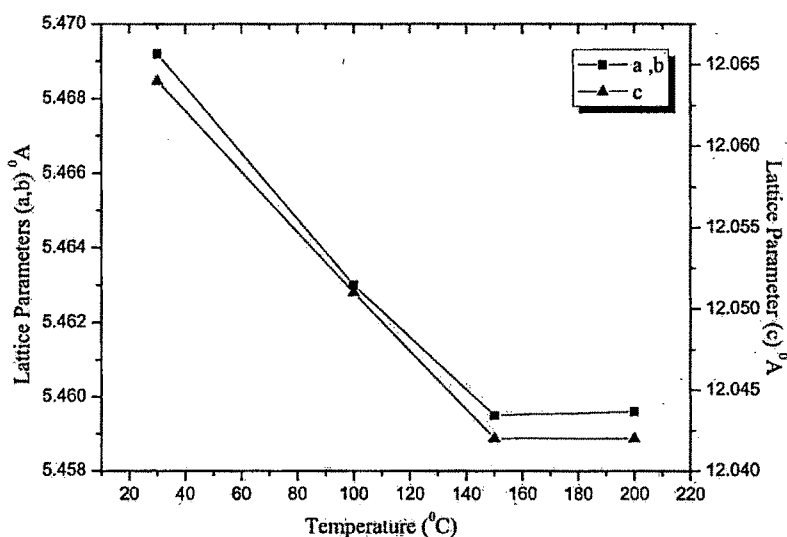


Figure 3.7.3 Effect of synthesis Temperature on Lattice Parameters of $\text{PbWO}_4:\text{Ce}$

We have plot the graph which shows the variation of lattice parameter as a function of Temperature for Cerium doped PbWO_4 synthesized at different temperature. Figure 3.7.3 shows the graph of Temperature verses Lattice parameter by taking the values tabulated in Table 3.9. As we can see from the table that, all PbWO_4 samples except prepared at 200 °C exhibit little amount of raspite phase. Lattice parameter (a,b) is highest for sample prepared at room temperature which decreases with increase in temperature up to 150 °C and then remains constant up to 200°C. Lattice parameter (c) also follows the same behaviour. Lattice parameter (c) is also highest for sample prepared at room temperature which decreases with increase in temperature up to 150 °C and then remains constant up to 200°C. Possible explanation for this can be given as follow. At room temperature nucleation and crystal growth occurs at very low temperature and so at room temperature Cerium was not able to replace Pb^{2+} . With increase in temperature more amount of Ce^{3+} ions substitute well Pb^{2+} ions in

PbWO_4 lattice and induce Pb^{2+} vacancy in order to keep the charge neutral. As ionic radius of Ce^{3+} ion is 0.103 nm which is slightly smaller than that of Pb^{2+} (0.120 nm). Hence with substitution of Ce^{3+} ion at Pb^{2+} site which increases with increase in temperature lattice parameter are decreases with increase in temperature.

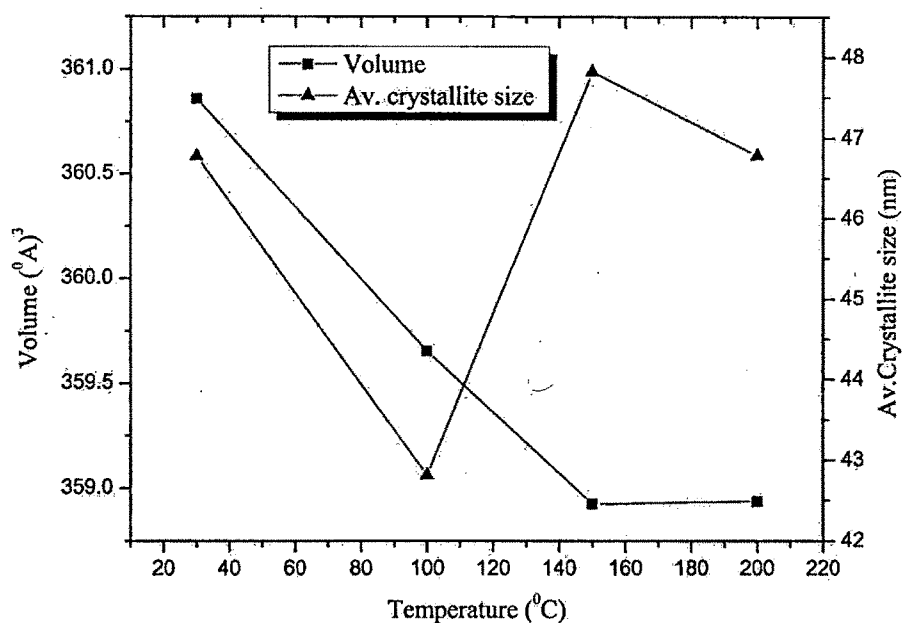


Figure 3.7.4 Effect of synthesis Temperature on Volume and Average Crystallite size of $\text{PbWO}_4:\text{Ce}$

We have also plot the graph which shows the variation of unit cell volume and average crystallite size as a function of Temperature. Figure 3.7.4 shows graph of Temperature verses unit cell volume and average crystallite size by taking the values tabulated in Table 3.9. Unit cell volume is highest for sample prepared at room temperature which decreases with increase in temperature up to 150 °C and then remains constant up to 200 °C. This can explain only the basis of substitution of Ce^{3+} ion on Pb^{2+} site decrease lattice parameters and hence unit cell volume. Average crystallite size is lowest for sample prepared 100 °C and almost remains same for

remaining samples. It well known that increase of temperature promotes a raise in the average crystallite size or particle size [25].

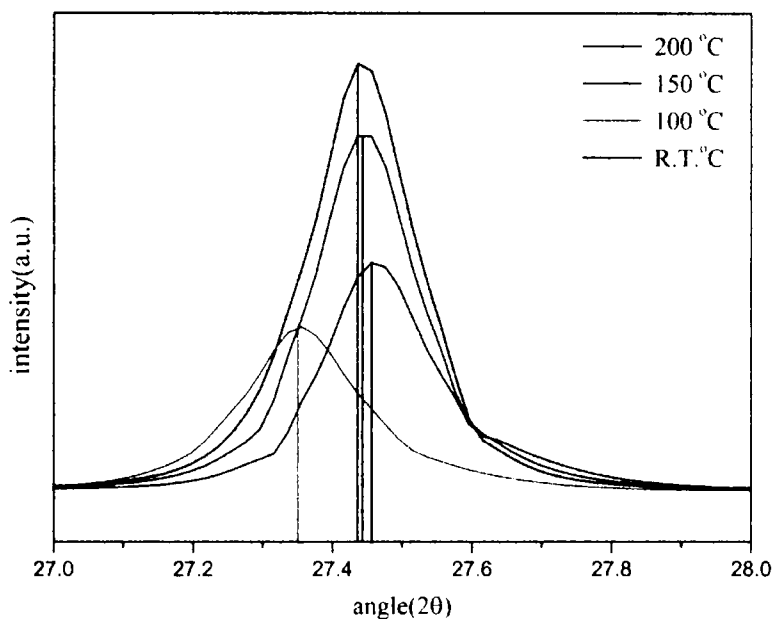


Figure 3.7.5 Shift of (112) peak of PbWO₄:Ce synthesized at different temperature

Figure 3.7.5 shows the shift of reflection peak (112) for different temperature towards higher angle suggests that the cell parameters of as-synthesized products could decrease with Ce³⁺ doping. The peak position of the PbWO₄: Ce samples synthesized at room temperature, 150°C and 200°C is almost same so lattice parameters of these samples should close to each other and smaller than the sample prepared at 100°C. This can be verified by values given in Table 3.9.

3.8 Effect of Cerium doping on structural properties of PbWO₄

There is only one report has been done on structural and optical properties of Cerium doped PbWO₄ by Yan Fang et al using wet chemical method [8]. Very few literatures are available in which affect of Ce³⁺ doping on luminescence property of PbWO₄ reported but effect of Ce³⁺ doping on crystal structure at different temperature is not reported till date. We have already discussed the effect Ce³⁺ at different temperatures. In this section comparison of XRD spectra of undoped and Cerium doped PbWO₄ at three individual 100°C, 150°C and 200°C temperatures is done. The XRD reflection spectra of undoped and Cerium doped PbWO₄ synthesized different temperatures are shown in Figure 3.8.1.

All XRD reflection peaks are indexed to a tetragonal scheelite (stolzite) phase with space group I4₁/a and monoclinic raspite phase with space group P2₁/a. The identification of raspite phase peaks for all samples are marked with symbol (*). The formation of Tungstic acid H₂WO₄.nH₂O, other tungsten oxide hydrates WO₃.nH₂O and unwashed impurity of Na₂WO₄, Ce₂(WO₄)₃, PbO, and Pb(OH)₂ were not observed, which reveals that the doping of Ce³⁺ at different temperatures does not change the crystal structure or induce a new phase.

Comparing XRD graphs of undoped and Cerium doped PbWO₄ samples prepared at 100°C, 150°C and 200°C following observations can be derived. Sample prepared at 100°C temperature contains highest amount of raspite phase compared to samples prepared at 150°C and 200°C temperatures. With increase of temperature from 100°C to 200°C percentage of raspite phase of PbWO₄ decreases. This indicates that at higher temperature stolzite phase with Tetragonal crystal structure dominates over raspite phase with monoclinic structure. In another words with increase in

temperature probability of raspite phase to convert into stolzite phase irreversibly increases. Conversion from raspite to stolzite is completed at 200°C temperatures and single phase PbWO_4 is produced.

It is also inferred from the XRD spectra that with Cerium doping, intensity of peaks representing raspite phase decreases and intensity of peaks representing stolzite phase increases. This behaviour is observed in all the samples for all the temperatures. Thus we can conclude that along with temperature doping of cerium also play an important role to decrease the amount of raspite phase and increase the amount of stolzite phase with increase in temperature.

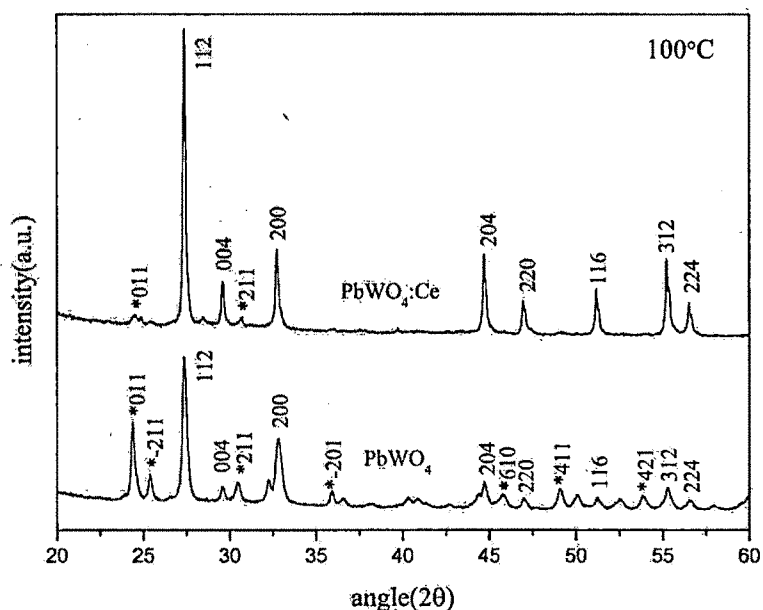


Figure 3.8.1 XRD spectra of PbWO_4 and $\text{PbWO}_4:\text{Ce}$ synthesized at 100°C.

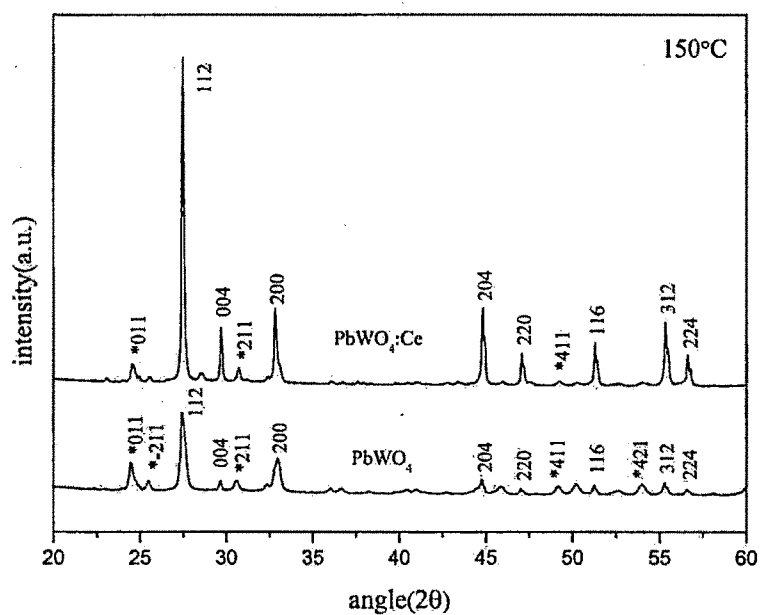


Figure 3.8.2 XRD spectra of PbWO_4 and $\text{PbWO}_4:\text{Ce}$ synthesized at 150°C.

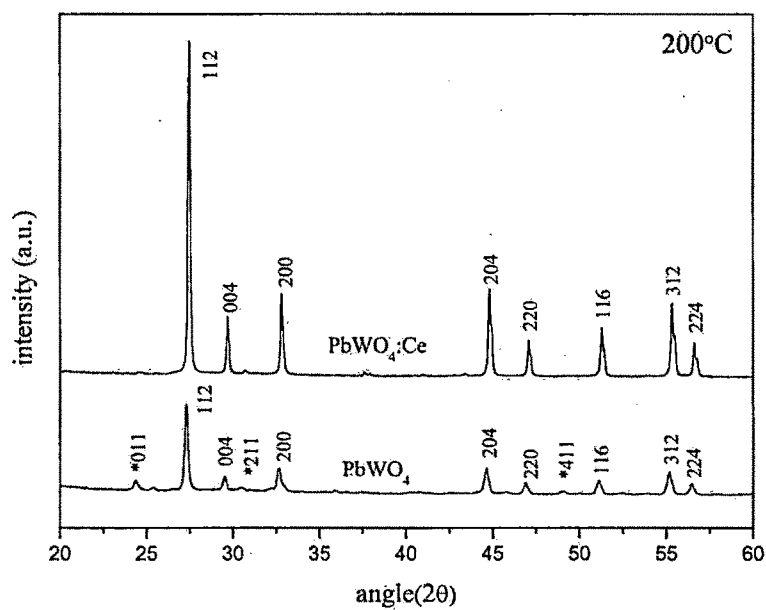


Figure 3.8.3 XRD spectra of PbWO_4 and $\text{PbWO}_4:\text{Ce}$ synthesized at 200°C

Table 4.0 Summary of phase identified, lattice parameters, unit cell volume and average crystallite size of undoped and Cerium doped PbWO_4 prepared at different Temperature.

Temp (°C)	Product	Phase	Lattice Parameter (Å)			Volume (Å) ³	Average crystallite size (nm)
			a	b	c		
100	PbWO_4	stolzite	5.4637	5.4637	12.051	359.74	28.27
		raspite	13.561	4.977	5.561	375.09	
	$\text{PbWO}_4\text{:Ce}$	stolzite	5.4630	5.4630	12.042	359.38	42.81
		raspite	13.555	4.976	5.556	375.33	
150	PbWO_4	stolzite	5.4595	5.4595	12.057	359.37	24.76
		raspite	13.496	4.985	5.579	375.34	
	$\text{PbWO}_4\text{:Ce}$	stolzite	5.4584	5.4584	12.042	358.78	47.82
		raspite	13.555	4.976	5.561	375.09	
200	PbWO_4	stolzite	5.4602	5.4602	12.049	359.23	36.32
		raspite	13.552	4.985	5.563	375.82	
	$\text{PbWO}_4\text{:Ce}$	stolzite	5.4596	5.4596	12.042	358.94	46.78

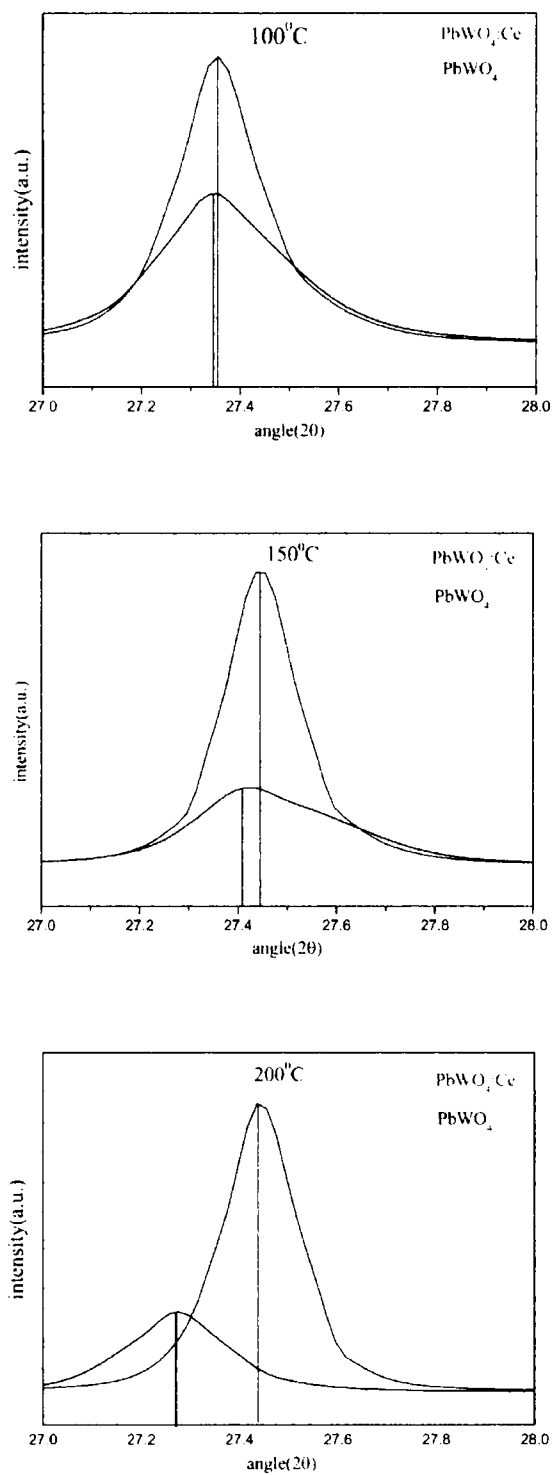


Figure 3.8.4 Shift of (112) peak of undoped and Cerium doped PbWO_4 prepared at different Temperature.

The cell parameters, unit cell volume and average crystallite size of undoped and Cerium doped PbWO_4 crystals for different temperatures were also investigated and the results are listed in Table 4.0. It is found from the table that the values of lattice parameters decreased and average crystallite size increase more than 50% with the introduction of Cerium for all the temperatures. Incorporation of Cerium in to PbWO_4 host lattice also decreases the unit cell volume. The appearance of these interesting phenomena is previously discussed and attributed: firstly due to the substitution Ce^{3+} for Pb^{2+} in the PbWO_4 crystal lattice induced the formation of Pb^{2+} vacancies to keep the charge neutral. Secondly, the ion radius of Ce^{3+} (0.103 nm) is slightly smaller than that of Pb^{2+} (0.120 nm). The Ce^{3+} ions would go into PbWO_4 crystal lattice well. The Ce^{3+} ions are likely to enter PbWO_4 crystal lattice to substitute Pb^{2+} sites considering that the ionic radius of Ce^{3+} (0.103 nm) is smaller than that of Pb^{2+} (0.120 nm) So the lattice parameters of Cerium doped PbWO_4 could be undoubtedly reduced. As reported for the La-doped PbWO_4 , the cell parameters decrease with increasing La^{2+} content [28]; a similar trend was also observed in results of our experiments.

Figure 3.8.4 shows the shift toward higher angle of reflection peaks suggested that the cell parameters of as-synthesized products could decrease with Ce^{3+} doping for the sample synthesized at 100 °C. The similar change can be seen in for the sample synthesized at 150 °C and 200°C also in Figure 3.8.4. The decrease in lattice parameter can also be confirmed from the Table 4.0. Distance between peak positions of undoped and Cerium doped PbWO_4 is increases with increase in the temperature, corresponding variation in lattice parameters can also be seen from Table 4.0.

References

- [1] Wei Zhao, Xinyu Song, Guozhu Chen, Guangru Tian and Sixiu Sun, *Materials Letters* 63, 285–288, 2009.
- [2] Biao Liu, Shu-Hong Yu, Linjie Li, Qiao Zhang, Fen Zhang and Ke Jiang, *Angew. Chem.* 116, 4849–4854, 2004.
- [3] Guangyu Chen, Liangbao Yang and Jinhuai Liu, *Cryst. Res. Technol.* 44, 7, 736–740, 2009.
- [4] Titipun Thongtem, Sulawan Kaowphong and Somchai Thongtem, *Ceramics International* 35, 1103–1108, 2009.
- [5] Jun Geng, Jun-Jie Zhu and Hong-Yuan Chen, *Crystal Growth & Design*, Vol.6, No.1, 2006.
- [6] Jun Geng, Yinong L, Dujuan Lu and Jun-Jie Zhu, *Nanotechnology* 17, 2614–2620, 2006.
- [7] Jun Geng, Dujuan Lu, Jun-Jie Zhu and Hong-Yuan Chen, *J. Phys. Chem. B* 110, 13777-13785, 2006.
- [8] Yan Fang, Ying Xiong, Yuanlin Zhou, Jinxiang Chen, Kaiping Song, Yi Fang and Xulan Zhen, *Solid State Sciences* 11, 1131–1136, 2009.
- [9] Xian-Luo Hu and Ying-Jie Zhu, *Langmuir* 20, 1521-1523, 2004.
- [10] Xiaoyan He and Minhua Cao, *Nanotechnology* 17, 3139–3143, 2006.
- [11] Di Chen, Guozhen Shen, Kaibin Tang, Zhenhua Liang and Huagui Zheng, *J. Phys. Chem. B*, 108, 11280-1284, 2004.
- [12] Changhua An, Kaibin Tang, Guozhen Shen, Chunrui Wang and Yitai Qian, *Materials Letters* 57, 565–568, 2002.
- [13] Thresiamma George, Sunny Joseph, Anu Tresa Sunny and Suresh Mathew, *J Nanopart Res* 10, 567–575, 2008.

- [14] Jinhu Yang, Conghua Lu, Hong Su, Jiming Ma, Humin Cheng and Limin Qi, *Nanotechnology* 19, 035608, 2008.
- [15] Guangjun Zhou, Mengkai Lu, Feng Gu, Dong Xu and Duorong Yuan, *Journal of Crystal Growth* 276,577–582, 2005.
- [16] Guangjun Zhou, Mengkai Lu, Benyu Su, Feng Gu, Zhiliang Xiu, Shufen Wang, *Optical Materials* 28,1385–1388, 2006.
- [17] Chunhua Zheng, Chenguo Hu, Xueyan Chen, Hong liu, Yufeng Xiong, Jing Xu, Buyong Wana and Linyong Huang, *CrystEngComm*, 12, 3277–3282, 2010.
- [18] Guizhen Wang, Chuncheng Hao, *Materials Research Bulletin* 44, 418–421, 2009.
- [19] Jeong Ho Ryu, Sang-Mo Koo, Dong Suk Chang, Jong-Won Yoon, Chang Sung Lim and Kwang Bo Shim, *Ceramics International* 32,647–652, 2006.
- [20] Hua Tang, Changsheng Li, Haojie Song, Xiaofei Yang and Xuehua Yan, *CrystEngComm*, 13, 5119, 2011.
- [21] C. Suryanarayana, M.G. Norton, *X-ray Diffraction: A Practical Approach*, Plenum Press, New York, 1998.
- [22] M. Kobayashi, Y. Usuki, M. Ishii, N. Senguttuvan, K. Tanji, M. Chiba, A. Hark, H. Takano, M. Nikl, P.Bohacek, S. Baccaro, A. Cecilia, M. Diemoz, A. Vedda and M. Martini, *Nucl. Instrum. Methods Phys. Res. A* 465, 428, 2001.
- [23] D.Tawde, M.Srinivas & K.V.R.Murthy, *physics status solidi a*, Vol.208, Issue 4, 2011, 803- 807.
- [24] D.Tawde, Dhaval Modi, M.Srinivas and K.V.R. Murthy, manuscript accepted to be published in *International Journal of Luminescence and its Applications*, 2012.
- [25] Jun Geng et al., *Crystal Growth & Design*, Vol. 6, No.1, 2006.
- [26] G. Zhou, M. Lu, F. Gu, D. Xu, D. Yuan, *J. Cryst. Growth* 276, 577, 2005.
- [27] L.S. Cavalcante , J.C. Sczancoski , V.C. Albarici , J.M.E. Matos , J.A. Varela , E.

Long , *Materials Science and Engineering B* 150,18–25, 2008.

[28] S. Takai, S. Touda, K. Oikawa, K. Mori, S. Torii, T. Kamiyama, T. Esaka, *Solid State Ionics* 148, 123, 2002.